

# Deep neural network for Wannier function centers

Linfeng Zhang

*Program in Applied and Computational Mathematics,  
Princeton University, Princeton, NJ 08544, USA*

Mohan Chen

*CAPT, HEDPS, College of Engineering, Peking University, Beijing 100871, China*

Xifan Wu

*Department of Physics, Temple University, Philadelphia, PA 19122, USA*

Han Wang\*

*Laboratory of Computational Physics, Institute of Applied Physics and  
Computational Mathematics, Huayuan Road 6, Beijing 100088, China*

Weinan E

*Department of Mathematics and Program in Applied and Computational Mathematics,  
Princeton University, Princeton, NJ 08544, USA and  
Beijing Institute of Big Data Research, Beijing, 100871, P.R. China*

Roberto Car<sup>†</sup>

*Department of Chemistry, Department of Physics,  
Program in Applied and Computational Mathematics,  
Princeton Institute for the Science and Technology of Materials,  
Princeton University, Princeton, NJ 08544, USA*

We introduce a deep neural network (DNN) model that assigns the position of the centers of the electronic charge in each atomic configuration on a molecular dynamics trajectory. The electronic centers are uniquely specified by the unitary transformation that maps the occupied eigenstates onto maximally localized Wannier functions. In combination with deep potential molecular dynamics, a DNN approach to represent the potential energy surface of a multi-atom system at the ab-initio density functional level of theory, the scheme makes possible to predict the dielectric properties of insulators using samples and trajectories inaccessible to direct ab-initio molecular dynamics simulation, while retaining the accuracy of that approach. As an example, we report calculations of the infrared absorption spectra of light and heavy water at a dispersion inclusive hybrid functional level of theory, finding good agreement with experiment. Extensions to other spectroscopies, like Raman and sum frequency generation, are discussed.

PACS numbers:

In the last decade we have witnessed a large development of machine learning (ML) schemes for representing the potential energy surface (PES) of many-atom systems [1–11]. These approaches are trained with first-principle data, typically derived from electronic density functional theory (DFT) [12], and may boost the power of *ab initio* molecular dynamics (AIMD) simulations [13, 14] by greatly extending accessible size and time scales without losing accuracy and predictive power. The reduction of statistical errors made possible by larger and longer simulations leads to more accurate predictions of static and dynamic properties. In addition, it becomes possible to study rare events, such as, e.g., crystal nucleation, using enhanced sampling methods in simulations of *ab initio* quality [15], while typically these techniques could only be employed with numerically efficient empirical force-fields.

In this context, ML approaches have focused mostly

on representing the PES as a function of the nuclear coordinates. Electronic structure properties, accessible in AIMD simulations, have only rarely been considered [4, 16–20]. Important examples are the polarization and/or the polarizability, which are needed to model infrared, Raman, and sum frequency generation spectra of insulators. A general formalism for computing the polarization utilizes maximally localized Wannier functions (MLWFs) [21, 22], i.e. electronic orbitals with minimal spatial spread generated by a unitary transformation of the occupied orbital subspace within DFT. The centers of the corresponding distributions, the Wannier function centers (WFCs), allow us to map the electronic charge density onto a set of point charges. Then, the polarization can be defined as the dipole moment of the system of electronic and nuclear point charges. For finite systems, i.e. molecules or clusters, this is the observable dipole moment, but for infinite periodic systems the

dipole moment is defined modulo a quantum [23], and the polarization is not an observable physical property. For both finite and extended systems, however, the polarization correlation functions are well defined and physically meaningful, as they describe the linear response of the system to an external perturbation.

Here we show how to construct a deep neural network (DNN) model to represent the dependence of the WFCs on the molecular environment. The scheme, called deep WFC (DWFC), is an end-to-end model, in the sense that it does not use any *ad hoc* construction to go from the input atomic coordinates to the output WFC coordinates. Furthermore, the model is size extensive, preserves the symmetry of the system, and yields a polarization that varies continuously with the atomic coordinates.

In this paper, we specialize to liquid water, a system in which the WFCs can be uniquely associated to the individual molecules, but it would be straightforward to extend the model to situations in which the WFCs can only be associated to atoms. This would be necessary, for instance, when water ions, such as hydronium ( $\text{H}_3\text{O}^+$ ) and hydroxide ( $\text{OH}^-$ ), are present in solution (see e.g. Ref. [24]). In these situations, interconversion of neutral molecules and ions accompanies proton transfer events, and the identity of a molecular species in an MD trajectory is no longer well defined. Yet, the WFCs remain unambiguously associated to the oxygen atoms.

For any atomic configuration of an insulating system the WFCs are uniquely specified by a unitary transformation of the ground-state Kohn-Sham orbitals. We focus here on the valence electrons only, and use pseudopotentials to describe their interaction with the atomic nuclei plus frozen core electrons. As expected from the principle of nearsightedness of the electronic matter [25, 26], we find that in liquid water the WFCs of a molecule depend only on the configuration of that molecule and its near neighbors.

We validate the methodology by showing that DWFC and AIMD predictions for the molecular dipole moment and the WFC-atom pair correlation functions are practically indistinguishable. To perform spectral calculations we combine DWFC with deep potential molecular dynamics (DPMD), an efficient ML scheme to generate nuclear trajectories of *ab initio* quality [9, 10]. DWFC locates the WFCs at all the nuclear configurations visited by DPMD, giving access to the dynamic evolution of the polarization and its time correlation functions. We demonstrate this feature by calculating the infrared spectra of liquid  $\text{H}_2\text{O}$  and  $\text{D}_2\text{O}$  at a hybrid functional level of theory with greatly reduced statistical errors compared to direct AIMD simulations.

In the DWFC scheme for neat water, we assign 2 hydrogens (H) and 4 WFCs to each oxygen (O) site labelled by the index  $i$ . Let  $\mathcal{N}_{r_c}^i = \{j, r_{ij} < r_c\}$  be the index set of the atoms  $j$  neighboring oxygen  $i$  within a cutoff radius  $r_c$ . The chemical species of atom  $j$  can be either O

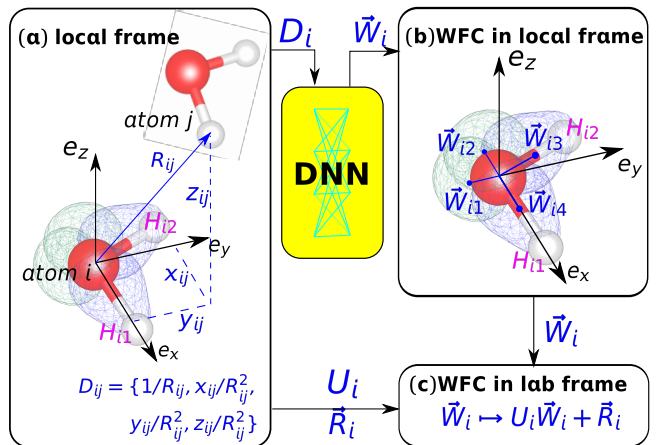


FIG. 1: (Color online) Schematic plot of the DWFC model for WFCs in liquid water. (a) Definition of the local frame and local generalized coordinates. Atom  $i$  is a generic oxygen atom and atom  $j \in \mathcal{N}_{r_c}^i$  is a generic neighbor of atom  $i$ .  $(e_x, e_y, e_z)$  defines the local frame of atom  $i$ . The oxygen  $i$  and the two hydrogens  $H_{i1}$  and  $H_{i2}$  belong to the same water molecule. We use  $H_{i1}$  to denote the hydrogen that is closer to the oxygen  $i$ .  $e_x$  is along the  $\text{O}_i\text{-H}_{i1}$  bond.  $e_z$  is perpendicular to the plane of the water molecule.  $e_y$  is the cross product of  $e_z$  and  $e_x$ .  $(e_x, e_y, e_z)$  forms a local rotation matrix  $U_i$  which maps the coordinates of  $j$  in the laboratory frame to those in the local frame.  $(x_{ij}, y_{ij}, z_{ij})$  are the Cartesian components of the vector  $\mathbf{R}_{ij}$  in this local frame.  $R_{ij}$  is the length of  $\mathbf{R}_{ij}$ . The neural network input  $\mathbf{D}_{ij} \equiv \{1/R_{ij}, x_{ij}/R_{ij}^2, y_{ij}/R_{ij}^2, z_{ij}/R_{ij}^2\}$  contains full coordinate information of atom  $j$ . We first sort the neighbors of atom  $i$  according to their chemical species, e.g. oxygens first and then hydrogens. Within each species we sort the atoms in ascending order of distances  $R_{ij}$ . We use  $\mathbf{D}_i$  to denote the sorted set of input data for site  $i$ . (b) Locations of the 4 WFCs,  $\mathbf{W}_{ia}$  ( $a = 1, 4$ ). The DNN takes the set  $\mathbf{D}_i$  in input and gives the set  $\mathbf{W}_i = \{\mathbf{W}_{ia}, a = 1, 4\}$  in output. The order of the four WFCs is fixed in the local frame. (c) Using the coordinates of site  $i$  and the rotation matrix  $U_i$  constructed in (a), the coordinates of the WFCs are transformed to the laboratory frame.

or H. Our goal is to construct a map from the coordinates of atoms  $i$  and  $j$  to 12 numbers, the coordinates of 4 WFCs. The symmetry constraints taken into account here are slightly different from those to model the PES within DPMD [9, 10]. The PES is *invariant* under translation, rotation, and identical particle permutation, while the WFCs are *equivariant*, i.e., they translate and rotate when the atomic positions are translated and rotated, guaranteeing a continuous evolution of the molecular dipoles. We achieve this goal by introducing a local frame for the  $i$ -th oxygen,  $\text{O}_i$ , in which the DNN converts input atomic coordinates into output WFC coordinates that are transformed back to the laboratory frame. In the local frame we sort the set  $\mathcal{N}_{r_c}^i$  in ascending order of distance from  $\text{O}_i$  and specify a corresponding order

for the WFCs. As shown in Fig. 1, the  $i$ -th local frame is defined by oxygen  $O_i$  and its two nearest hydrogens,  $H_{i1}$  and  $H_{i2}$ . The ordered local coordinate information is encoded in  $\mathbf{D}_{ij} = \{1/R_{ij}, x_{ij}/R_{ij}^2, y_{ij}/R_{ij}^2, z_{ij}/R_{ij}^2\}$ , wherein  $x_{ij} = x_j - x_i$ ,  $y_{ij} = y_j - y_i$ ,  $z_{ij} = z_j - z_i$ , in terms of the Cartesian coordinates of atoms  $i$  and  $j$  in the local frame,  $R_{ij} = \sqrt{x_{ij}^2 + y_{ij}^2 + z_{ij}^2}$ , and the factor  $1/R_{ij}$  reduces the weight of the more distant atoms. The ordered set  $\mathbf{D}_i \equiv \{\mathbf{D}_{ij}, j \in \mathcal{N}_{r_c}^i\}$  serves as the input of a DNN, which returns 12 numbers in output through multiple hidden layers. In each hidden layer a linear transformation is applied to the input data, followed by the action of a non-linear function called the activation function. In the final step from the last hidden layer to the WFC positions, i.e.  $\mathbf{W}_{i1}$ ,  $\mathbf{W}_{i2}$ ,  $\mathbf{W}_{i3}$ , and  $\mathbf{W}_{i4}$ , only the linear transformation is applied. We indicate by  $\mathbf{W}_i = \{\mathbf{W}_{i1}, \mathbf{W}_{i2}, \mathbf{W}_{i3}, \mathbf{W}_{i4}\}$  the ordered set of the WFCs associated to the molecule  $i$  and by  $f^\gamma$  the map  $\mathbf{D}_i \mapsto \mathbf{W}_i$ , where  $\gamma$  are the parameters of the linear transformations. We use the hyperbolic tangent for the activation function and adopt 4 hidden layers with decreasing number of nodes, i.e., 200, 100, 50, and 20 nodes, respectively, from the innermost to the outermost layer.

To apply our protocol we first identify the four WFCs associated to  $O_i$  and then we order them in an equivariant way. The first task is accomplished by selecting the WFCs whose distance from  $O_i$  is less than 0.8 Å. The second task is accomplished by identifying  $\{\mathbf{W}_{i1}, \mathbf{W}_{i2}, \mathbf{W}_{i3}, \mathbf{W}_{i4}\}$  as shown in Fig. 1 (b). In the local frame,  $\mathbf{W}_{i1}$  and  $\mathbf{W}_{i2}$  lie approximately along the  $\mathbf{e}_z$  axis, which is perpendicular to the molecular plane defined by  $O_i$ ,  $H_{i1}$ , and  $H_{i2}$ . Thus  $\mathbf{W}_{i1}$  and  $\mathbf{W}_{i2}$  represent the centers of the lone pairs.  $\mathbf{W}_{i3}$  and  $\mathbf{W}_{i4}$ , which lie approximately along the two bonding O-H directions, represent the centers of the bond pairs. To assign a unique order to the four WFCs we assign  $\mathbf{W}_{i1}$  ( $\mathbf{W}_{i2}$ ) to the positive (negative)  $\mathbf{e}_z$  direction, and assign  $\mathbf{W}_{i3}$  ( $\mathbf{W}_{i4}$ ) to the  $O_i$ - $H_{i1}$  ( $O_i$ - $H_{i2}$ ) bond. With this assignment  $f^\gamma$  is a well-defined one-to-one map in the  $i$ -th environment. The parameters  $\gamma$  are determined by training, i.e., an optimization process that minimizes a loss function, which we define here to be the mean square difference between the DWFC prediction and the training data. The Adam stochastic gradient descent method [27] is adopted for the optimization.

To construct the DPMD and DWFC models for liquid water, we used a dataset generated by a path-integral (PI) AIMD simulation of 64  $H_2O$  molecules subject to periodic boundary conditions [28]. The electronic structure was described within DFT using the PBE0-TS functional that combines the hybrid functional PBE0 [29] with the self-consistent TS functional for dispersion interactions [30]. The training data were taken from an equilibrated PI-AIMD trajectory lasting 8 ps at isothermal-isobaric conditions with  $P = 1$  bar and  $T = 300$  K. The

calculated equilibrium density was 1.01 g/cm<sup>3</sup>. The integration of the equations of motion for the Feynman paths used the i-PI code [31] interfaced with the CP module of Quantum Espresso [32, 33] to compute on the fly the ground-state of the electrons within Born-Oppenheimer conditions. The i-PI code used 8 beads for a converged representation of the Feynman paths with the generalized Langevin equation [34]. DPMD training was made with the DeePMD-kit [35] using the smooth version of the model, introduced in Ref. [11], to eliminate the small discontinuities associated to sharp cutoff and permutations in the original model [10]. The smooth version has similar accuracy, but unlike the original model, it allows us to generate the long microcanonical trajectories that are needed to evaluate classical time correlation functions with small statistical errors.

To train the DWFC model we used 95000 snapshots (from a total of 105000 snapshots), randomly selected along the PI-AIMD trajectory. The rest of the PI-AIMD snapshots were used for testing. In addition, we used DWFC to predict the WFC evolution along an independent classical AIMD trajectory (with the same DFT approximation) at  $T = 330$  K and a simulation box fixed at the experimental density at room temperature [36]. In our model the only adjustable parameter is the cutoff radius  $r_c$ . We found that the error of the model decreases with increasing  $r_c$  and converges to a small finite value when  $r_c$  is large enough to include the first shell of neighboring molecules. With our adopted choice, i.e.  $r_c = 4.5$  Å, the root mean square error (RMSE) in the predicted WFC positions is 0.0033 (0.0049) Å in our classical (PI) AIMD trajectories. As in Ref. [37] we define the dipole moment of the  $i$ -th molecule in terms of the atom and WFC positions in the laboratory frame by  $\boldsymbol{\mu}_i = e(6\mathbf{R}_{O_i} + \mathbf{R}_{H_{i1}} + \mathbf{R}_{H_{i2}} - 2\sum_{a=1}^4 \mathbf{R}_{W_{ia}})$ , where  $e$  denotes the electronic charge. The RMSE of the predicted dipole moments is 0.032 (0.038) Debye, approximately 1% of the average dipole value, in the classical (PI) trajectories. We notice that only PI-AIMD trajectories have been used for training. The good performance of DWFC for the classical trajectory at  $T = 330$  K indicates some transferability of the model to different thermodynamic conditions.

Next, we use DWFC to access the WFC evolution over long DPMD trajectories. We report in Fig. 2 the atom-WFC and dipole distributions for a quantal (PI-DPMD) and a classical (DPMD) trajectory, each one 1 ns long, at the thermodynamic conditions of the original simulations used to train and test the DWFC model. We also report in the same figure the same quantities along two corresponding but much shorter AIMD trajectories. The agreement is very good.

Finally, we illustrate the usefulness of the DPMD+DWFC scheme for spectral calculations, by calculating the IR absorption spectra of liquid  $H_2O$  and  $D_2O$  for a sample of 512 molecules under periodic

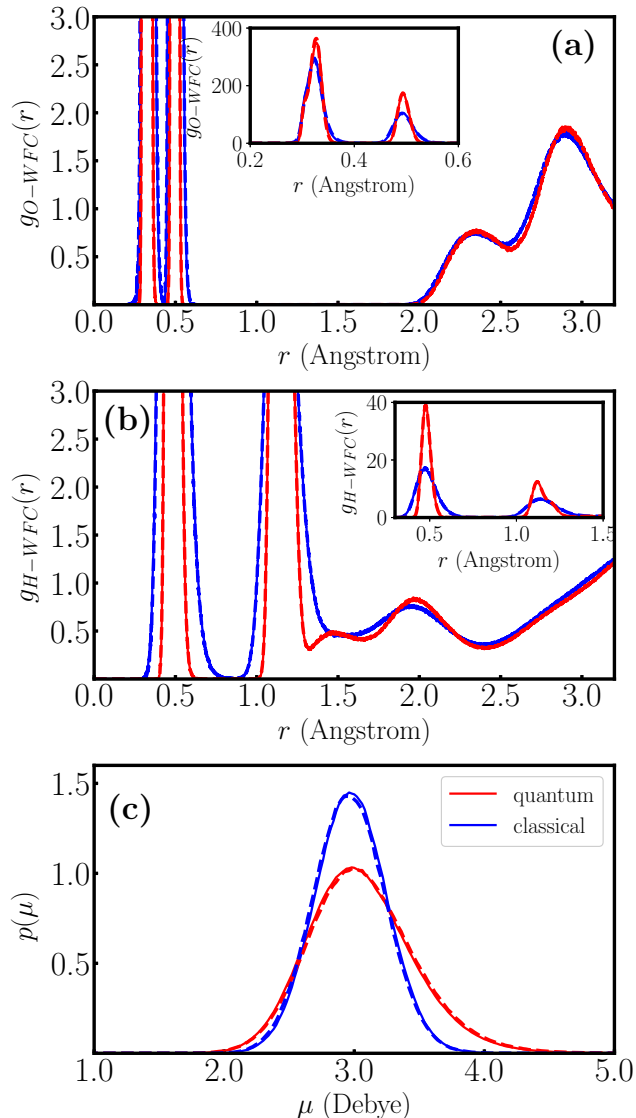


FIG. 2: (Color online) Distribution functions associated to the WFCs on quantum (PI) (red) and classical (blue) trajectories: (a) O-WFC pair correlation function  $g_{O-WFC}(r)$ ; (b) H-WFC pair correlation function  $g_{H-WFC}(r)$ ; (c) probability distribution of the magnitude of the molecular dipole ( $\mu$ ). Solid (dashed) lines refer to the DWFC (AIMD) data (see text).

boundary conditions. We use two microcanonical trajectories lasting 500 ps each, for H<sub>2</sub>O and D<sub>2</sub>O, corresponding to an average temperature of  $\sim 300$  K at the equilibrium density of the original PI-AIMD simulation at  $T = 300$  K. The frequency dependent IR absorption coefficient per unit length,  $\alpha(\omega)$ , is given within linear response theory by the Fourier transform of the time correlation function of the polarization

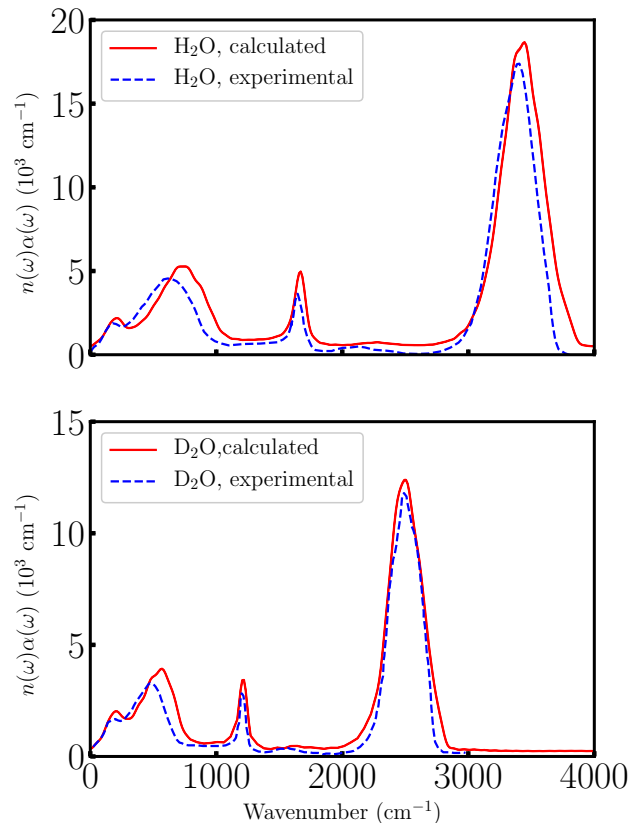


FIG. 3: (Color online) IR absorption spectra of H<sub>2</sub>O (upper panel) and D<sub>2</sub>O (lower panel). The continuous red lines report DPMD+DWFC calculations (512 molecules, 0.5 ns long microcanonical trajectories). The variance of the spectra estimated with different DNN initializations (see text) is smaller than the line width. The dashed blue lines report experimental data for H<sub>2</sub>O at 298 K (from Ref. [38]) and for D<sub>2</sub>O at 295 K (from Ref. [39]).

$\mathbf{M} = \sum_i \mu_i$ , according to:

$$\alpha(\omega) = \frac{2\pi\omega^2\beta}{3cVn(\omega)} \int_{-\infty}^{+\infty} dt e^{-i\omega t} \langle \mathbf{M}(0) \cdot \mathbf{M}(t) \rangle, \quad (1)$$

where  $n(\omega)$  is the refractive index, which is a constant taken from experiment within the relevant frequency range,  $V$  is the volume,  $\beta = 1/k_B T$  is the inverse temperature, and  $k_B$  is the Boltzmann factor. The calculated spectra for light and heavy water are reported in Fig. 3 together with the corresponding experimental observations. To further check the quality of the DWFC model, we calculated the variance of the IR spectra predicted by DNN models that differ among themselves only in the initialization of the network parameters  $\gamma$ . Due to the highly non-linear dependence of  $f^\gamma$  on the network pa-

rameters, different initializations result in multiple local minima in the landscape of the loss function, originating an ensemble of minimizers, each one of which specifies a different DNN model. The variance of the predictions within this ensemble of DNNs is an intrinsic property of these models and can be used as an indicator of their accuracy [16, 40–42]. Using this criterion and a normally distributed random choice of the initial parameters, we obtain a relative variance uniformly smaller than 1%, i.e., smaller than the line width of the spectra in Fig. 3.

Overall, the agreement of theory and experiment is good. The spectra are characterized by 3 main features, i.e., in order of decreasing frequencies, H stretching, molecular bending, libration and network modes (see, e.g., analysis in Ref. [37]). The low frequency feature comprises a broader feature at higher frequencies attributed to librations, and a narrower and less prominent feature at lower frequencies attributed to hydrogen bond network modes. The calculated H<sub>2</sub>O spectrum is blue-shifted by  $\sim 45 \text{ cm}^{-1}$  relative to experiment in the stretching region. The corresponding shift is barely noticeable in D<sub>2</sub>O. Relative to experiment, the theoretical spectra of both H<sub>2</sub>O and D<sub>2</sub>O, exhibit a sharper bending peak and far IR features that are blue shifted and have larger intensity.

The small differences between theory and experiment in Fig. 3 should be attributed to the adopted DFT approximation and the use of a classical instead of a quantum autocorrelation function in Eq. 1. Zhang et al. [43] showed that the hybrid functional PBE0 yields a substantially better IR spectrum than semilocal functionals like PBE [44]. Our simulation used PBE0 with dispersion corrections for a better description of the liquid structure [36]. Quantum fluctuations affect both the static and the dynamic response of water, but while static correlation functions can be evaluated without approximation with path integral simulations, dynamic correlation functions require integrals of complex functions, whose exact evaluation is a major challenge for statistical simulation methods. Recently, quantum IR correlations have been calculated for water using approximate methods like ring polymer [45] and centroid [45, 46] MD, indicating that quantum corrections tend to red shift the spectral features predicted by classical calculations. Further studies of these issues will be facilitated by methods like DPMD and DWFC, which greatly improve the statistical quality of *ab initio* simulations.

In summary, DWFC is a powerful tool to parametrize the dependence of the centers of electronic charge from the coordinates of the atoms in their environment. The approach developed here could be extended to deal with other electronic properties, such as, e.g., the molecular polarizability tensors  $\alpha_{\delta\sigma}^i = \frac{\partial \mu_{i\delta}}{\partial E_\sigma}$ , where  $\mu_{i\delta}$  is the  $\delta$ -Cartesian component of the molecular dipole  $\boldsymbol{\mu}_i$  and  $E_\sigma$  is the  $\sigma$ -component of a uniform electric field applied to the system. A deep neural network could be

constructed to represent the dependence of  $\alpha_{\delta\sigma}^i$  on the  $i$ -th molecular environment  $\{\mathbf{R}_i, \mathbf{R}_j, j \in \mathcal{N}_{r_c}^i\}$  specified by a cutoff radius  $r_c$ , similarly to what we have done here for the WFCs. In this way we could compute Raman [47] and sum frequency generation spectra [48, 49]. The ability to access the combined evolution of the nuclear coordinates and the associated polarization in simulations of large systems over long time scales should also open the way to direct MD studies of ferroelectric phase transitions without relying on simplified model Hamiltonians [50–52]. Finally, we should mention that many popular ML schemes [1, 2, 8, 11], including DPMD, represent the PES by a sum of many-body atomic terms  $E_i(\{\mathbf{R}_i, \mathbf{R}_j, j \in \mathcal{N}_{r_c}^i\})$ , which are short ranged in spite of being trained with AIMD data that contain long range electrostatics. Explicit inclusion of long range electrostatic effects in DPMD may be necessary in some applications, such as, e.g., when one is interested in the longitudinal-transverse splitting of the optical phonons in ionic materials. In these situations, the DWFC scheme could be used to define a PES representation that includes explicitly the electrostatic energy of the system of nuclear and electronic point charges.

The work of L. Z., X. W., W. E, and R.C. was conducted at the Center Chemistry in Solution and at Interfaces (CSI) funded by the DOE Award DE-SC001934. The work of L. Z and W. E is supported in part by a gift from iFlytek to the Princeton University as well as ONR grant N00014-13-1-0338. The work of H.W. is supported by the NSFC under Grant 11871110, the National Key Research and Development Program of China under Grants 2016YFB0201200 and 2016YFB0201203. We are grateful for computing time provided by the Terascale Infrastructure for Groundbreaking Research in Science and Engineering (TIGRESS) High Performance Computing Center and Visualization Laboratory at Princeton University.

---

\* Electronic address: wang\_han@iapcm.ac.cn

† Electronic address: rcar@princeton.edu

- [1] J. Behler and M. Parrinello, *Physical Review Letters* **98**, 146401 (2007).
- [2] A. P. Bartók, M. C. Payne, R. Kondor, and G. Csányi, *Physical Review Letters* **104**, 136403 (2010).
- [3] M. Rupp, A. Tkatchenko, K.-R. Müller, and O. A. VonLilienfeld, *Physical Review Letters* **108**, 058301 (2012).
- [4] G. Montavon, M. Rupp, V. Gobre, A. Vazquez-Mayagoitia, K. Hansen, A. Tkatchenko, K.-R. Müller, and O. A. Von Lilienfeld, *New Journal of Physics* **15**, 095003 (2013).
- [5] V. Botu, R. Batra, J. Chapman, and R. Ramprasad, *The Journal of Physical Chemistry C* **121**, 511 (2016).
- [6] S. Chmiela, A. Tkatchenko, H. E. Sauceda, I. Poltavsky, K. T. Schütt, and K.-R. Müller, *Science Advances* **3**,

- e1603015 (2017).
- [7] K. Schütt, P.-J. Kindermans, H. E. S. Felix, S. Chmiela, A. Tkatchenko, and K.-R. Müller, in *Advances in Neural Information Processing Systems* (2017) pp. 992–1002.
- [8] J. S. Smith, O. Isayev, and A. E. Roitberg, *Chemical Science* **8**, 3192 (2017).
- [9] J. Han, L. Zhang, R. Car, and W. E, *Communications in Computational Physics* **23**, 629 (2018).
- [10] L. Zhang, J. Han, H. Wang, R. Car, and W. E, *Physical Review Letters* **120**, 143001 (2018).
- [11] L. Zhang, J. Han, H. Wang, W. Saidi, R. Car, and W. E, in *Advances in Neural Information Processing Systems 31*, edited by S. Bengio, H. Wallach, H. Larochelle, K. Grauman, N. Cesa-Bianchi, and R. Garnett (Curran Associates, Inc., 2018) pp. 4441–4451.
- [12] W. Kohn and L. J. Sham, *Physical Review* **140**, A1133 (1965).
- [13] R. Car and M. Parrinello, *Physical Review Letters* **55**, 2471 (1985).
- [14] D. Marx and J. Hutter, *Ab initio molecular dynamics: basic theory and advanced methods* (Cambridge University Press, 2009).
- [15] L. Bonati and M. Parrinello, *Physical Review Letters* **121**, 265701 (2018).
- [16] M. Gastegger, J. Behler, and P. Marquetand, *Chemical Science* **8**, 6924 (2017).
- [17] A. Grisafi, D. M. Wilkins, G. Csányi, and M. Ceriotti, *Physical Review Letters* **120**, 036002 (2018).
- [18] A. Grisafi, A. Fabrizio, B. Meyer, D. M. Wilkins, C. Corminboeuf, and M. Ceriotti, *ACS Central Science* **5**, 57 (2018).
- [19] D. M. Wilkins, A. Grisafi, Y. Yang, K. U. Lao, R. A. DiStasio Jr., and M. Ceriotti, *Proceedings of the National Academy of Sciences*, 201816132 (2019).
- [20] A. Chandrasekaran, D. Kamal, R. Batra, C. Kim, L. Chen, and R. Ramprasad, *NPJ Computational Materials* **5**, 22 (2019).
- [21] N. Marzari and D. Vanderbilt, *Physical Review B* **56**, 12847 (1997).
- [22] N. Marzari, A. A. Mostofi, J. R. Yates, I. Souza, and D. Vanderbilt, *Reviews of Modern Physics* **84**, 1419 (2012).
- [23] R. Resta, *Reviews of Modern Physics* **66**, 899 (1994).
- [24] M. Chen, L. Zheng, B. Santra, H.-Y. Ko, R. A. DiStasio Jr., M. L. Klein, R. Car, and X. Wu, *Nature Chemistry*, 1 (2018).
- [25] W. Kohn, *Physical Review Letters* **76**, 3168 (1996).
- [26] E. Prodan and W. Kohn, *Proceedings of the National Academy of Sciences* **102**, 11635 (2005).
- [27] D. Kingma and J. Ba, in *Proceedings of the International Conference on Learning Representations (ICLR)* (2015).
- [28] B. Santra, H.-Y. Ko, L. Zhang, R. A. DiStasio Jr., and R. Car, “Nuclear Quantum Effects in Liquid Water and Ice,” (in prep.).
- [29] C. Adamo and V. Barone, *The Journal of Chemical Physics* **110**, 6158 (1999).
- [30] A. Tkatchenko and M. Scheffler, *Physical Review Letters* **102**, 073005 (2009).
- [31] M. Ceriotti, J. More, and D. E. Manolopoulos, *Computer Physics Communications* **185**, 1019 (2014).
- [32] P. Giannozzi, S. Baroni, N. Bonini, M. Calandra, R. Car, C. Cavazzoni, D. Ceresoli, G. L. Chiarotti, M. Cococcioni, I. Dabo, A. Dal Corso, S. de Gironcoli, S. Fabris, G. Fratesi, R. Gebauer, U. Gerstmann, C. Gougoussis, A. Kokalj, M. Lazzeri, L. Martin-Samos, N. Marzari, F. Mauri, R. Mazzarello, S. Paolini, A. Pasquarello, L. Paulatto, C. Sbraccia, S. Scandolo, G. Sclauzero, A. P. Seitsonen, A. Smogunov, P. Umari, and R. M. Wentzcovitch, *Journal of Physics: Condensed Matter* **21**, 395502 (2009).
- [33] P. Giannozzi, O. Andreussi, T. Brumme, O. Bunau, M. B. Nardelli, M. Calandra, R. Car, C. Cavazzoni, D. Ceresoli, M. Cococcioni, N. Colonna, I. Carnimeo, A. D. Corso, S. d. Gironcoli, P. Delugas, R. A. DiStasio Jr., A. Ferretti, A. Floris, G. Fratesi, G. Fugallo, R. Gebauer, U. Gerstmann, F. Giustino, T. Gorni, J. Jia, M. Kawamura, H.-Y. Ko, A. Kokalj, E. Küçükbenli, M. Lazzeri, M. Marsili, N. Marzari, F. Mauri, N. L. Nguyen, H.-V. Nguyen, A. Otero-de-la Roza, L. Paulatto, S. Poncè, D. Rocca, R. Sabatini, B. Santra, M. Schlipf, A. P. Seitsonen, A. Smogunov, I. Timrov, T. Thonhauser, P. Umari, N. Vast, X. Wu, and S. Baroni, *Journal of Physics: Condensed Matter* **29**, 465901 (2017).
- [34] M. Ceriotti, D. E. Manolopoulos, and M. Parrinello, *The Journal of Chemical Physics* **134**, 084104 (2011).
- [35] H. Wang, L. Zhang, J. Han, and W. E, *Computer Physics Communications* **228**, 178 (2018).
- [36] R. A. DiStasio Jr, B. Santra, Z. Li, X. Wu, and R. Car, *The Journal of Chemical Physics* **141**, 084502 (2014).
- [37] W. Chen, M. Sharma, R. Resta, G. Galli, and R. Car, *Physical Review B* **77**, 245114 (2008).
- [38] J. E. Bertie and Z. Lan, *Applied Spectroscopy* **50**, 1047 (1996).
- [39] J. E. Bertie, M. K. Ahmed, and H. H. Eysel, *The Journal of Physical Chemistry* **93**, 2210 (1989).
- [40] J. S. Smith, B. Nebgen, N. Lubbers, O. Isayev, and A. E. Roitberg, *The Journal of Chemical Physics* **148**, 241733 (2018).
- [41] L. Zhang, H. Wang, and W. E, *The Journal of Chemical Physics* **148**, 124113 (2018).
- [42] L. Zhang, D.-Y. Lin, H. Wang, R. Car, and W. E, *Physical Review Materials* **3**, 023804 (2019).
- [43] C. Zhang, D. Donadio, F. Gygi, and G. Galli, *Journal of Chemical Theory and Computation* **7**, 1443 (2011).
- [44] J. P. Perdew, K. Burke, and M. Ernzerhof, *Physical Review Letters* **77**, 3865 (1996).
- [45] O. Marsalek and T. E. Markland, *The Journal of Physical Chemistry Letters* **8**, 1545 (2017).
- [46] G. R. Medders and F. Paesani, *Journal of Chemical Theory and Computation* **11**, 1145 (2015).
- [47] Q. Wan, L. Spanu, G. A. Galli, and F. Gygi, *Journal of Chemical Theory and Computation* **9**, 4124 (2013).
- [48] S. Mukamel, *Principles of nonlinear optical spectroscopy*, Vol. 41 (1998) pp. 591–592.
- [49] Y. Nagata and S. Mukamel, *Journal of the American Chemical Society* **132**, 6434 (2010).
- [50] R. Resta and D. Vanderbilt, in *Physics of Ferroelectrics* (Springer, 2007) pp. 31–68.
- [51] V. Srinivasan, R. Gebauer, R. Resta, and R. Car, in *AIP Conference Proceedings*, Vol. 677 (AIP, 2003) pp. 168–175.
- [52] D. Vanderbilt and W. Zhong, *Ferroelectrics* **206**, 181 (1998).